A Surface Flux Parameterization Based on the Vertically Averaged Turbulence Kinetic Energy

CHANGAN ZHANG AND DAVID A. RANDALL

Department of Atmospheric Science, Colorado State University, Fort Collins, Colorado

CHIN-HOH MOENG

National Center for Atmospheric Research, Boulder, Colorado

MARK BRANSON

Department of Atmospheric Science, Colorado State University, Fort Collins, Colorado

KERRY A. MOYER

Woods Hole Oceanographic Institution, Woods Hole, Massachusetts

QING WANG

Naval Postgraduate School, Monterey, California

(Manuscript received 11 January 1996, in final form 9 May 1996)

ABSTRACT

A new bulk transfer formulation for the surface turbulent fluxes of momentum, heat, and moisture has been developed by using the square root of the vertically averaged turbulent kinetic energy (TKE) in the atmospheric boundary layer as a velocity scale, in place of the mean wind speed. The new parameterization utilizes the surface radiative (skin) temperature instead of the temperature at a "roughness height." Field observations and large-eddy simulation (LES) results were used to develop the parameterization. It has been tested using an independent dataset from the First ISLSCP (International Satellite Land Surface Climatology Project) Field Experiment (FIFE). The predicted surface momentum flux compares very well with the observations, despite the fact that the data used for developing the new parameterization have a very different roughness length from the independent FIFE data. This shows that the parameterization can represent a wide range of surface roughness boundary conditions. The predicted sensible and latent heat fluxes also agree well with the FIFE observations, although the predicted surface sensible heat flux is somewhat less than observed at the FIFE site. The diurnal cycles of the predicted surface sensible heat and latent heat fluxes correspond very well with the observations in both magnitude and phase.

1. Introduction

The surface turbulent fluxes of sensible heat, moisture, and momentum are determined in numerical models through the use of a bulk aerodynamic formula, such as

$$(\overline{w'\theta'})_S = |\mathbf{V}_b| C_h(\Theta_0 - \Theta_a). \quad (1)$$

Here w is the vertical velocity, θ is potential temperature, overbars and primes denote averages and departures from those averages, subscript S denotes a level near the surface, $|\mathbf{V}_b|$ is the grid-averaged wind speed at a level within the surface layer, C_h is a transfer coefficient, subscript 0 denotes the lower boundary, and subscript a denotes a level within the surface layer. Although (1) is quite familiar, and its use is quite routine, it actually involves a number of ambiguities and it can be applied in a model only after several somewhat arbitrary choices have been made.

The starting point for any discussion of (1) is the recognition that it is not derived from more general equations; it is really nothing more than the definition of C_h. This definition is motivated by the empirical facts that the turbulent flux of a property (in this case, the potential temperature) across the earth's surface is associated with a "difference" in that property be-

Corresponding author address: Dr. Changan Zhang, Colorado State University, Department of Atmospheric Science, Fort Collins, CO 80523-1371.
E-mail: changan@chasm.atmos.colostate.edu

tween the boundary and the air, and is promoted by the near-surface wind.

A first step toward practical use of (1) is to choose the levels at which to measure the flux itself, the mean wind speed $|\mathbf{V}_b|$, the "boundary" potential temperature Θ_0, and the "air" potential temperature Θ_a. The flux typically changes slowly with height near the surface, so the precise level to which it is referred is not too critical. The wind speed and potential temperature often change very rapidly with height near the surface, however, so that $|\mathbf{V}_b|$ and the difference $\Theta_0 - \Theta_a$ can be quite sensitive to the levels at which $|\mathbf{V}_b|$, Θ_0, and Θ_a are defined.

Under neutral conditions, the mean wind vanishes at the "aerodynamic roughness height," z_0, which ranges from a millimeter or so over the ocean to several meters over forests. This is in fact the definition of the aerodynamic roughness height. The mean wind increases logarithmically upward (again under neutral conditions) for $z > z_0$. Following Thom (1972), Θ_0—the potential temperature of the lower boundary—is sometimes defined at a "roughness height for temperature," z_t, which is typically several orders of magnitude smaller than the aerodynamic roughness height, and is a function of the flow regime, and is strongly dependent on the surface conditions (Garratt 1992). Brutsaert and Sugita (1991 and 1992), Beljaars and Holtslag (1991), Beljaars (1994), Stull (1994), and Sun and Mahrt (1995) used the surface radiative temperature in place of the near-surface air temperature, and introduced a "radiative roughness height."

In practice, most numerical models set the boundary potential temperature equal to the potential temperature of the sea surface[1] or soil surface, instead of trying to work out the potential temperature at the roughness height for temperature. Here, $|\mathbf{V}_b|$ and Θ_a are often referred to levels a few meters above the surface (e.g., Louis 1979). Recently, the conceptual utility of a roughness height for temperature has called this into question (L. Mahrt 1996, personal communication).

Once these choices have been made, (1) can be used to derive values of C_h empirically. The dependencies of C_h on stability and surface roughness are parameterized empirically with the aid of similarity theory (e.g., Stull 1988). Many surface flux parameterizations are based on the Monin–Obukhov surface layer similarity theory (Businger et al. 1971; Dyer 1974; Paulson 1970), according to which the transfer coefficients for momentum, heat, and moisture can be expressed as functions of the atmospheric stability and the surface roughness length (Garratt 1977; Garratt and Francey 1978; Louis 1979; Sommeria 1988; Brutsaert and Sugita 1990 and 1991; Beljaars and Holtslag 1991; Beljaars 1994; Stewart 1995). It then becomes possible to use (1) in a model, to determine the surface potential temperature flux, provided that $|\mathbf{V}_b|$, Θ_0, and Θ_a are known somehow. For this purpose, most numerical models provide at least one thin model layer (i.e., finite-difference layer) adjacent to the surface; the top of this lowest model layer typically lies below the top of the planetary boundary layer (PBL).

This approach has some weaknesses. First, thin layers contain very little mass and so have little inertia. The layer properties can be altered very quickly, so that arguably it makes more sense to use (1) to determine Θ_a from $(\overline{w'\theta'})_S$, rather than the reverse. In addition, it is necessary to determine the turbulent fluxes not only at the lower edges of such layers (e.g., at the surface) but also at their upper edges, because these still lie within the PBL.

Deardorff (1972) advocated a rather different approach. He recommended parameterization of the PBL in a numerical model through the incorporation of a bulk boundary layer model, such as a mixed-layer model. In this approach, depth of the PBL is introduced as a parameter, and is explicitly predicted by the model. The vertically averaged properties of the PBL (e.g., winds, temperature, and humidity) are also predicted. Deardorff defined $|\mathbf{V}_b|$ and Θ_a in (1) to be vertical averages through the depth of the PBL. This means that he defined C_h in terms of such averages. He suggested a suitable parameterization for C_h, based in part on large-eddy simulations. His parameterization made C_h depend significantly on the surface roughness.

Deardorff's approach has some advantages. Over a large fraction of the earth's surface, the pressure thickness of the PBL is 50 mb or more. Such a relatively thick layer has considerable dynamic and thermodynamic inertia. Essentially by definition, it is identically the PBL whose vertically averaged properties are altered by the surface fluxes, so it is very convenient for a model to predict those averages directly.

In keeping with the traditional approach, Deardorff used the vertically averaged wind speed as a "velocity scale" in (1). This causes difficulties when the mean wind goes to zero while the surface fluxes remain finite. When the wind is calm, free convection drives the turbulent fluxes, and the convective velocity can be used as a velocity scale (Deardorff 1970). The problem of determining the fluxes under weak wind conditions was actually considered from the earliest days of large-scale numerical modeling (e.g., Langlois and Kwok 1969), and has been addressed by many investigators including Deardorff (1972), Liu et al. (1979), and Godfrey and Beljaars (1991). The study of Miller et al. (1992) served to rekindle interest in this subject. Miller et al. found that weak wind conditions occur frequently over the tropical oceans in the ECMWF (European Centre for Medium-Range Weather Forecasts) model and that a satisfactory parameterization of surface exchange under weak-wind conditions is needed to produce a re-

[1] Even sea surface temperature is somewhat ill defined since the water temperature can change rapidly within the upper few centimeters.

alistic tropical general circulation. Their improved parameterization led to an increased surface latent heat flux, which had a strongly beneficial impact on the simulated tropical circulation and precipitation distribution. Mahrt and Sun (1995) derived the bulk aerodynamic formulation, in terms of subgrid-scale averaging and time averaging, and obtained results similar to those of Godfrey and Beljaars (1991).

Recently, Stull (1994) suggested replacing the wind speed in (1) by a velocity scale that is a measure of the intensity of the turbulence. He also followed Deardorff (1972) by using the vertically averaged PBL properties for $|\mathbf{V}_b|$ and Θ_a. He used the surface radiative temperature (the temperature that when raised to the fourth power and multiplied by the Stefan–Boltzman constant yields the upwelling longwave flux) for Θ_0. Stull also suggested that, with these definitions, the surface transfer coefficients should not depend significantly on the surface roughness. He pointed out that under convective conditions the surface resistance is negligible compared with the resistance from the surface layer to the mixed layer and that the momentum transfer coefficients observed by Yamada (1976) show no dependency on the surface roughness length, even though the transfer coefficients calculated from surface-layer similarity do vary strongly with changing roughness (suitably nondimensionalized).

This paper extends the work of Deardorff (1972) and Stull (1994) by presenting a new bulk transfer parameterization of the surface turbulent fluxes of momentum, heat, and moisture. The transfer coefficients are defined using the vertically averaged turbulence kinetic energy (TKE) as the velocity scale, the vertically averaged PBL properties, and the surface radiative temperature. TKE is generated by both shear and buoyancy fluxes, and will always exist as long as there are turbulent fluxes. This makes the square root of the TKE a good choice for the velocity scale.

In this paper, we occasionally compare our approach to that of Deardorff (1972) for two reasons. First, we have been using Deardorff's approach in our modeling work for many years (e.g., Randall 1976; Suarez et al. 1983). Second, Deardorff's approach, like the one we present here, is expressly designed for use with a bulk boundary layer model.

Our new surface flux parameterization is described in section 2. The datasets used for developing the parameterization are described in section 3. Section 4 presents the resulting parameterized transfer coefficients, and the results of tests based on an independent dataset. Section 5 gives the conclusions. Tests of the parameterization in a general circulation model will be described elsewhere.

2. Transfer coefficients for momentum and heat

We define the transfer coefficients for momentum C_M, heat C_T, and water vapor C_q using

$$-(\overline{u'w'})_S = e_M^{1/2} C_M |U_M|, \tag{2}$$

$$(\overline{w'\theta'})_S = e_M^{1/2} C_T (\Theta_S - \Theta_M), \tag{3}$$

and

$$(\overline{w'q'})_S = e_M^{1/2} C_q (q_S - q_M), \tag{4}$$

where e is the turbulent kinetic energy (TKE) and subscripts S and M denote the surface and vertically averaged boundary layer values, respectively; that is,

$$X_M = \frac{1}{Z_i} \int_0^{Z_i} X(z) dz, \tag{5}$$

where Z_i is the PBL depth. Although (2)–(4) are really nothing more than definitions of C_M, C_T, and C_q, they nevertheless have a very simple physical interpretation: to have a turbulent flux, there must be a surface–air difference of the property in question, and in addition there must be some turbulence kinetic energy. This can be contrasted with the corresponding interpretation of (1), which is that in order to have a turbulent flux, there must be a surface–air difference of the property in question, and in addition there must be a mean wind.

We can interpret the transfer coefficients C_M, C_T, and C_q as measures of the efficiency with which the TKE produces fluxes near the surface. As is well known, the turbulent velocity fluctuations near the surface have to be quasi-horizontal. On the other hand, vertical fluxes near the boundary must be associated with nonzero vertical velocity fluctuations there (e.g., Businger and Oncley 1990). The transfer coefficients measure how strong these near-surface vertical velocity fluctuations are, per unit $e_M^{1/2}$. It is therefore reasonable to expect that the static stability near the surface will affect the transfer coefficients.

The surface flux transfer coefficients C_M, C_T, and C_q in (2)–(4) must be empirically determined, presumably as functions of one or more nondimensional parameters. The nature of this parametric dependence is discussed later. We assume from this point on that $C_T = C_q$.

3. Data

We have used data from two different field studies and results from several large-eddy simulations, as outlined below. The data required are the surface fluxes of momentum and sensible heat, the vertically averaged PBL values of the wind components and potential temperature, the vertically averaged TKE, and the surface skin temperature. To compute vertical means over the PBL, it is also necessary to determine the PBL depth. We have not tried to analyze the moisture fluxes because of difficulties in determining the effective moisture availability associated with the soil and vegetation.

TABLE 1. Summary of the data for stable conditions.

No.	Z_i (m)	U_M (m s^{-1})	Θ_M (K)	Θ_S (K)	$\overline{w'\theta'}$ (K m s^{-1})	u_* (m s^{-1})	e_M (m^2 s^{-2})	Ri_B
1	300	12.8	290.8	289.6	−0.0071	0.33	0.238	0.0759
2	400	15.3	294.9	292.9	−0.0160	0.44	0.422	0.1160
3	200	7.8	294.6	291.1	−0.0079	0.18	0.071	0.3822
4	100	4.7	282.5	279.4	−0.0047	0.12	0.032	0.4806

a. Observed unstable cases

The data from BLX83, which was conducted near Chickasha, Oklahoma (35°N, 97°W), includes only "unstable" cases, with upward surface buoyancy fluxes. The data were processed and published by Stull (1994); see his Table 1. They were collected on flights of the Queen Air aircraft of the National Center for Atmospheric Research (NCAR). Mixed-layer mean values of the wind speed, potential temperature, and water vapor mixing ratio were computed for flight altitudes between $0.3Z_i$ and $0.7Z_i$. The depth of the boundary layer was determined from ground-based lidar observations. The surface turbulent fluxes of momentum, heat, and moisture were determined using the eddy correlation method, with instruments mounted on the aircraft, during its near-surface flights between $0.1Z_i$ and $0.3Z_i$. The surface radiative temperature was measured by a downward-looking radiometer mounted on the aircraft.

To estimate the vertically averaged TKE for the BLX83 data, we have used the results of Moeng and Sullivan (1994), who showed that a linear combination of the TKE dissipation rates associated with shear and buoyancy can adequately approximate the vertical distribution of the TKE in a variety of boundary layers ranging from near neutral to free convection conditions. They assumed that the total TKE dissipation rate ϵ is

$$\epsilon = \epsilon_S + \epsilon_B, \tag{6}$$

where ϵ_S is the dissipation rate due to the shear production of TKE and ϵ_B is the dissipation rate due to buoyancy production. These are diagnosed using

$$\epsilon_S = u_*^3\left(1 - \frac{z}{Z_i}\right)\frac{\phi_m}{kz}, \tag{7}$$

and

$$\epsilon_B = \frac{0.4w_*^3}{Z_i}, \tag{8}$$

where u_* and w_* are the surface friction velocity and the convective velocity scales, respectively. Here, $\phi_m = (1 - 15z/L)^{-1/4}$ is an empirical function for the unstable atmospheric surface layer (Businger et al. 1971), which is applied to both the surface and mixed layers. In (8), we have assumed that the downward entrainment-driven potential temperature flux at the top of the PBL is 20% of the upward surface potential temperature flux for the buoyancy-driven PBL (Tennekes 1973; Driedonks 1982; Moeng and Wyngaard 1988). The von Kármán constant, $k = 0.4$, was applied to (7), instead of $k = 0.35$ obtained by Businger et al. (1971). We found the estimated TKE values show very small differences by using either $k = 0.4$ or 0.35.

Following inertial range arguments, the total TKE dissipation rate ϵ can be written as

$$\epsilon = \frac{(2e)^{3/2}}{L_\epsilon}, \tag{9}$$

TABLE 2. Summary of the LES dataset.

No.	Z_i (m)	U_M (m s^{-1})	Θ_M (K)	Q_M (g kg^{-1})	Θ_o (K)	Q_o (g kg^{-1})	Potential temperature flux (K m s^{-1})	Moisture flux (g kg^{-1} m s^{-1})	u_* (m s^{-1})	w_* (m s^{-1})	e_M (m^2 s^{-1})	Ri_B
1	1021	7.70	302.0	13.4	305.6	15.0	0.24	0.097	0.570	2.014	1.907	−9.92
2	479	8.91	301.1	13.3	302.0	15.0	0.05	0.086	0.568	0.9280	0.6971	−0.687
3	486	9.23	300.6	13.7	301.2	15.0	0.03	0.060	0.555	0.786	0.6422	−0.436
4	465	9.85	300.3	14.0	300.3	15.0	0.00	0.035	0.492	0.000	0.5922	0.0027
5	462	10.10	300.3	14.1	300.3	15.0	0.00	0.030	0.536	0.000	0.5863	0.0030
6	1066	11.34	300.6	12.3	301.5	15.0	0.05	0.143	0.664	1.211	0.9744	−0.780
7	493	3.56	300.7	13.0	301.6	15.0	0.03	0.064	0.283	0.790	0.3774	−5.70
8	944	8.88	301.2	13.0	303.6	15.0	0.15	0.121	0.624	1.678	1.496	−4.04
9	1024	8.83	301.9	12.8	305.4	15.0	0.24	0.136	0.632	2.016	1.972	−7.07
10	1038	10.71	302.2	13.1	305.4	15.0	0.24	0.130	0.723	2.025	2.165	−4.24
11	1021	14.79	300.3	14.0	300.3	15.0	0.00	0.039	0.666	0.000	0.8233	0.0022

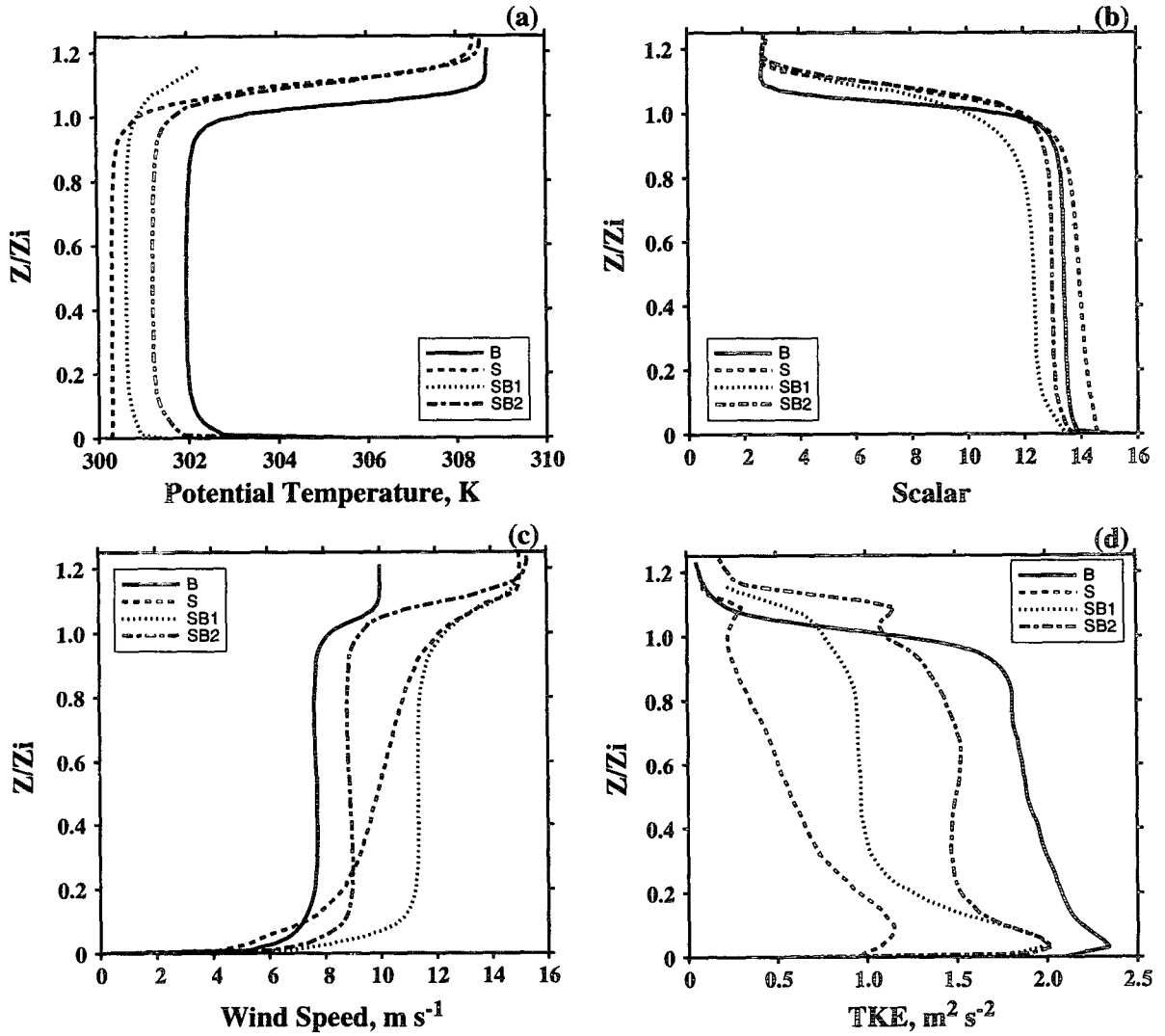

FIG. 1. A demonstration of the LES mean profiles of (a) potential temperature, (b) scalar, (c) wind speed, and (d) turbulence kinetic energy for buoyancy-driven (B), shear- and buoyancy-driven (SB), and shear-driven (S) boundary layers.

where L_ϵ characterizes the integral length scale of the dissipation rate. Combining (6)–(9), the TKE profile can be expressed as

$$e(z) = \frac{1}{2}\left(\frac{L_\epsilon}{Z_i}\right)^{2/3}\left[0.4w_*^3 + u_*^3(Z_i - z)\frac{\phi_m}{kz}\right]^{2/3}$$

$$= F\left(u_*, w_*, \frac{z}{Z_i}\right). \quad (10)$$

The result obtained for e is sensitive to L_ϵ. We used $L_\epsilon = 2.6Z_i$, which is in the range $2.5Z_i$–$3.0Z_i$ suggested by Moeng and Sullivan (1994).

b. Observed stable cases

The surface transfer coefficients for stable conditions have been computed using data taken from the paper of Lenschow et al. (1988), as listed in Table 1. The data was collected in May 1979 in central Oklahoma, in support of a subprogram of the Severe Environmental Storms and Mesoscale Experiment (SESAME). Most of the data are based on aircraft observations made using the NCAR Queen Air. Tethered balloon and acoustic sounder systems were also used. The observations were filtered, with high- and low-frequency cutoffs of 10 Hz and 0.01 Hz, respectively.

We have estimated the surface radiative temperature using the similarity formulation of Businger et al. (1971) and Dyer (1974),

$$\Theta_0 = \Theta_m - \frac{0.74\Theta_*}{k}\left[\ln\left(\frac{Z_m}{z_t}\right) + 6.35\frac{Z_m}{L}\right], \quad (11)$$

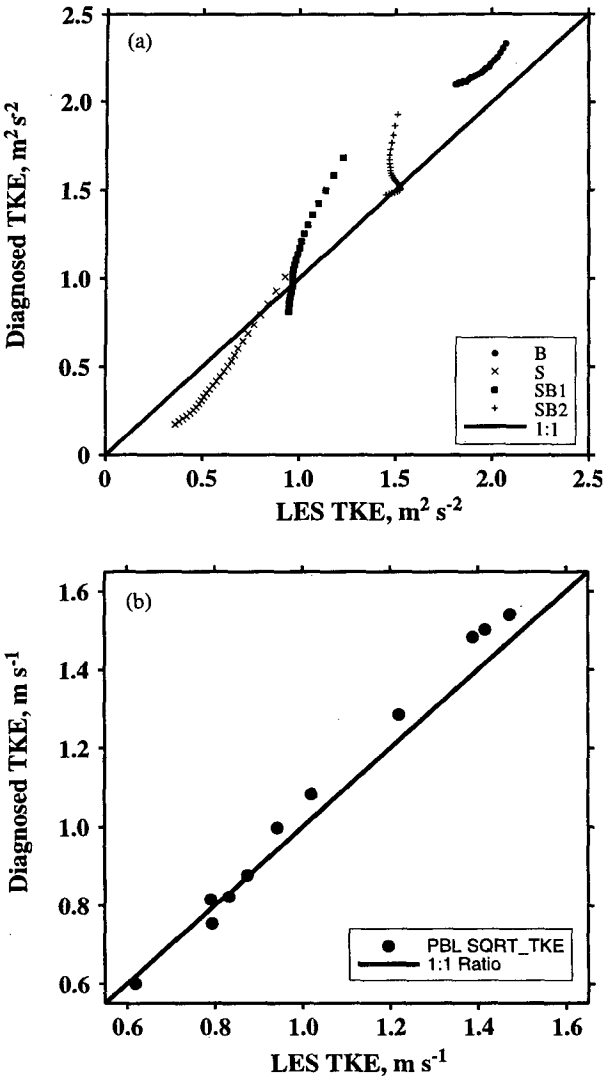

FIG. 2. Comparisons of the turbulent kinetic energy (TKE) as simulated by LES model and as predicted by the parameterization. (a) The profiles of the TKE for the 4 cases; (b) the square root of the vertically averaged TKE for 11 cases.

and the temperature profile in the interfacial sublayer based on laboratory observations (Liu et al. 1979),

$$\frac{\Theta_0 - \Theta_s}{\Theta_*} = 13.3[1 - e^{(-0.7z_t u_*/\nu/13.3)}]. \quad (12)$$

Here, Θ_0 is the surface air temperature at roughness height z_t, Θ_S is the surface temperature, $\Theta_* = -\overline{w'\theta_s'}/u_*$, is the potential temperature scale, $k = 0.4$ is von Kármán's constant, $L = -\bar{\Theta}_v u_*^3 \times [kg(\overline{w'\theta_v'})_s]^{-1}$ is the Monin–Obukhov length, and Θ_m is the potential temperature at height Z_m. We use $z_t = 0.11\nu/u_*$ because the roughness height is very close to the surface interfacial sublayer (Kondo 1975; Liu et al. 1979; Godfrey and Beljaars 1991); here $\nu = 1.46 \times 10^{-5}$ m^2 s^{-2} is the kinematic molecular viscosity of air.

To estimate the vertically averaged TKE of the stable atmospheric boundary layer, we modeled the TKE profile using an empirical function proposed by Lenschow et al. (1988), based on aircraft observations:

$$\frac{e(z)}{u_*^2} = 6\left(1 - \frac{z}{Z_i}\right)^{1.75}. \quad (13)$$

This is similar to the formula used by Caughey et al. (1979). The vertically averaged TKE can then be estimated by integrating (10) and (13) through the interior of the PBL, from the surface to the top of the atmospheric boundary layer (Z_i).

c. *Large-eddy simulations*

We have also used the results of large-eddy simulations (LESs) performed by C.-H. Moeng. The LES code was developed by Moeng (1984) and modified by Moeng and Wyngaard (1988). The Navier–Stokes equations are solved explicitly. The effects of unresolved motions are parameterized based on inertial-subrange theory. A total of 11 simulations are used in this study (Table 2), ranging from neutral to free convective cases, obtained by varying the large-scale pressure gradient and the prescribed surface heat flux.

Figure 1 shows four of the cases studied by Moeng and Sullivan (1994), to illustrate the mean PBL structures driven by buoyancy only (B), by shear (S), and by both buoyancy and shear (SB1 and SB2). The domain sizes are 3 km × 3 km × 1 km for the S and BS cases, and 5 km × 5 km × 2 km for the B case. All runs use 96 × 96 × 96 grid cells. For the mean profiles of potential temperature Θ and passive scalar Q, the B, S, and SB cases present a similar structure, that is, there is a clearly defined mixed layer above the surface layer and a well-defined inversion at the top of the PBL. The tracer Q has both surface and entrainment fluxes, similar to the moisture field. Flow visualizations show, however, that the S and B cases have quite different turbulent flow fields. The B case produces convective cells, while the S case generates more streaklike horizontal rolls along the direction of the wind shear (Moeng and Sullivan 1994). For the U profile, the B and SB cases have similar shapes, with strong wind shear within surface layer and a nearly constant wind speed in the mixed (outer) layer. On the other hand, the S case presents a much larger wind shear in the surface layer and an almost constant wind shear throughout the outer part of the boundary layer. This wind shear is of course necessary to maintain the turbulence kinetic energy for the shear-driven PBL.

The vertically averaged mean wind speed, potential temperature, tracer concentration, and surface fluxes are listed in Table 2. The mean wind speed, potential temperature, tracer concentration, and turbulence ki-

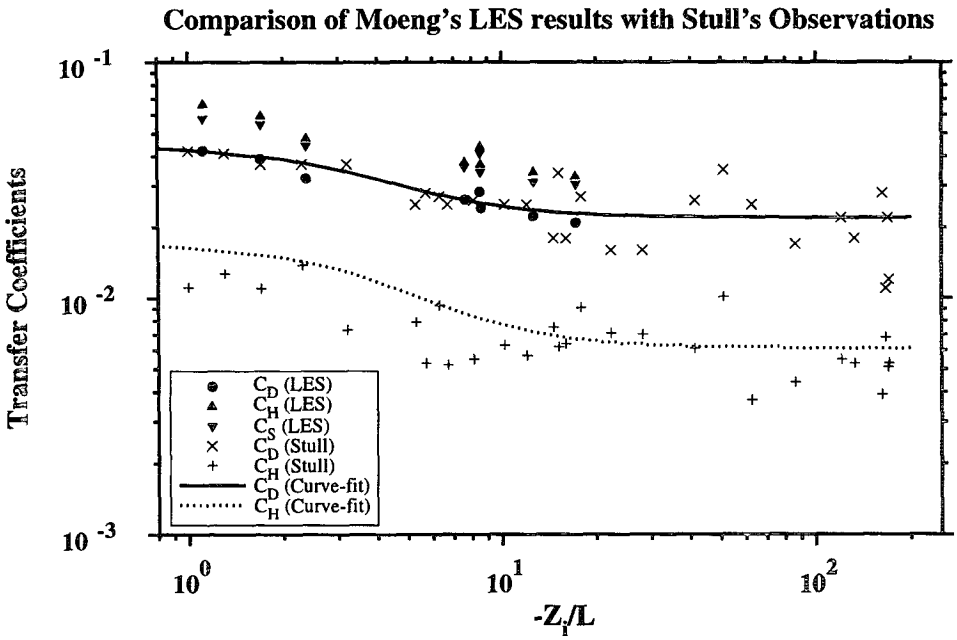

FIG. 3. Comparisons of the bulk transfer coefficients for momentum (C_D) and heat/moisture (C_H) between the LES and the field observations (Stull 1994). The solid and dotted lines are curve fits of the field observation data for C_D and C_H, respectively.

netic energy have been computed from the horizontal domain-averages of the LES results, by averaging from the surface to Z_i. The aerodynamic roughness height is $z_0 = 0.16$ m. The values of the potential temperature and tracer concentration at the aerodynamic roughness height, Θ_0 and Q_0, were computed from the corre-

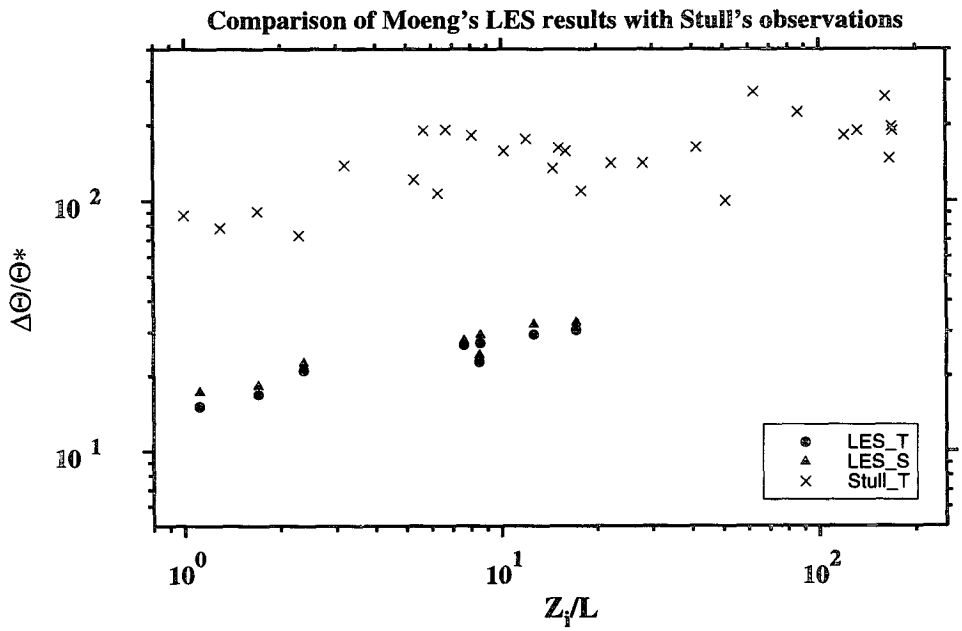

FIG. 4. A comparison of the normalized potential temperature differences between surface and the mixed-layer values. The LES (solid circle and triangle), and the field observations (crosses). LES_T denotes the temperature, and LES_S denotes the passive scalar.

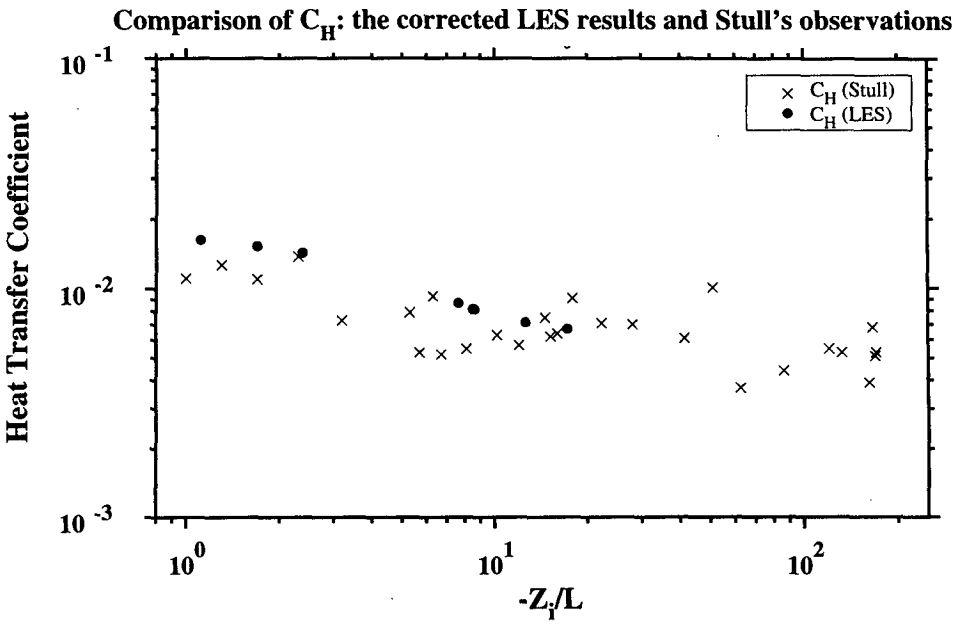

FIG. 5. A comparison of the heat transfer coefficients between the field observation and the LES results after the differences between the skin temperature and the roughness-height temperature have been corrected for.

sponding prescribed surface fluxes and simulated mean potential temperature and tracer concentration at the first model level, using the surface-layer similarity formulations.

As a check, we have compared the TKE diagnosed from (10) with that obtained directly from the LES. Figure 2a compares the TKE values at each height for the four PBL cases shown in Fig. 1, while Fig. 2b compares their vertically averaged values for all 11 LES cases. The average is taken between the surface to Z_i, before taking the square root. The diagnosed TKE agrees well with that obtained through LES, with slight underestimates of the low values and slight overestimates of the high values, which correspond to shear-driven and buoyancy-driven PBLs, respectively. As would be expected, the vertically averaged TKEs agree much better than the TKE profiles. The relative errors in the vertically averaged TKE range from 0.6% to 6.8%. The mean error is 4.3% for the 11 LES cases.

As a further check, we used the LES results to compute Stull's (1994) momentum and heat transfer coefficients, C_D and C_H, which are defined by

$$-(\overline{u'w'})_S = w_* C_D U_M, \tag{14}$$

and

$$(\overline{w'\theta'})_S = w_* C_H(\Theta_S - \Theta_M). \tag{15}$$

Here, $w_* = [(g/\theta_v)Z_i(\overline{w'\theta_v'})_S]^{1/3}$ is the convective velocity scale proposed by Deardorff (1970). Figure 3 shows a comparison of C_D and C_H, defined by (14) and (15), as obtained from the LES results and the observations of Stull (1994). The coefficients are plotted as functions of $\zeta = -Z_i/L$, where Z_i is the PBL depth and L is the Monin–Obukhov length. The solid and dotted lines are curve fits. The momentum transfer coefficients computed from the LES results (circles) agree very well with Stull's observations (crosses). In strong contrast, the observed C_H values are about five times smaller than those obtained from the LES results in the same stability range.

The reason for this huge discrepancy is that the temperature at the aerodynamic roughness height, Θ_0, was used in (15), to evaluate the heat transfer coefficients from the LES results, whereas the radiative skin temperature Θ_S is actually called for. As is well known, under convective conditions, Θ_0 is generally cooler than Θ_S (Paw U 1984; Choudhury 1985; Stull 1994; Sun and Mahrt 1995). This is why the values of C_H calculated from the LES results are larger than those observed. In Fig. 4, we present the normalized potential temperature differences, $(\Theta_0 - \Theta_M)/\Theta_*$ and $(\Theta_S - \Theta_M)/\Theta_*$, from the LES results and the observations, respectively. Both $(\Theta_0 - \Theta_M)/\Theta_*$ and $(\Theta_S - \Theta_M)/\Theta_*$ increase with increasing instability, but as expected the skin temperature is consistently warmer than the roughness-height temperature. The ratio of the two potential temperature differences is comparable to the ratio of the heat transfer coefficients obtained from the LES and the observations, as shown in Fig. 3.

Unfortunately, Θ_S is not available in the LES results; if it had been, we would of course have used it above.

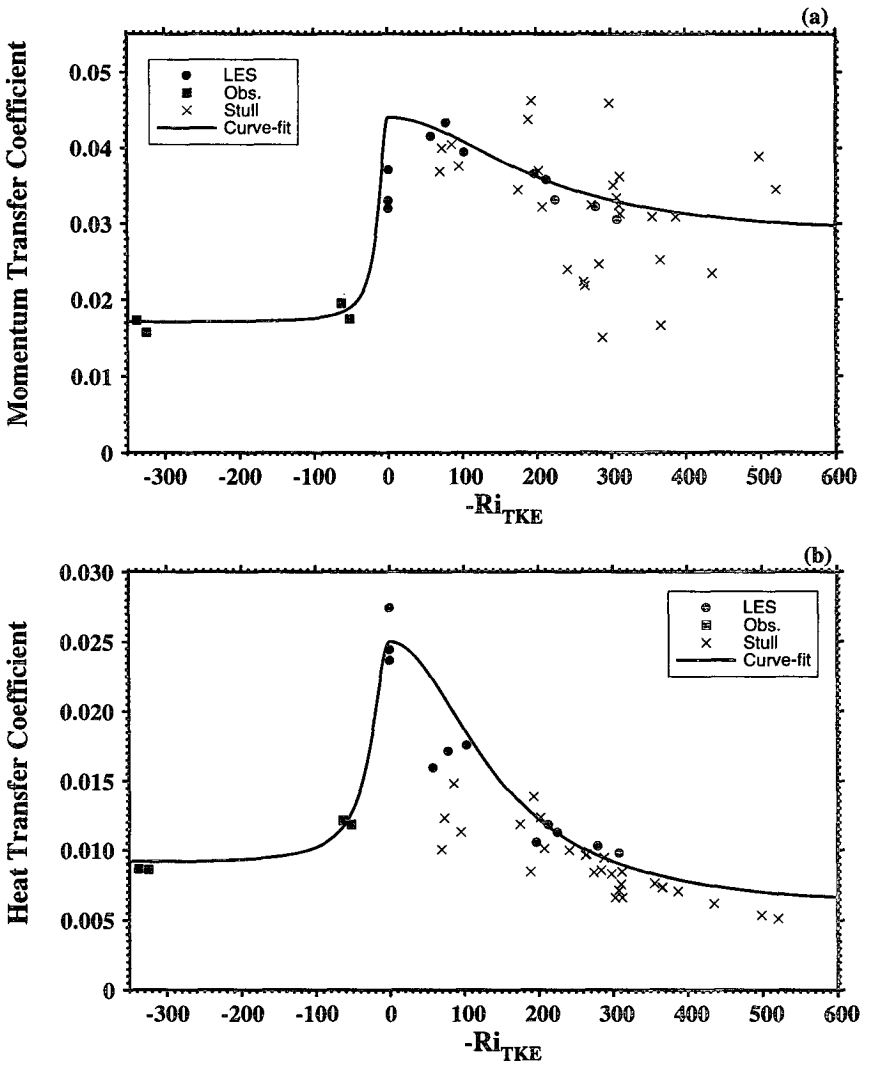

FIG. 6. Parameterized (a) surface momentum flux transfer coefficient C_M and (b) surface heat/moisture flux transfer coefficient C_T. Curves in (a) and (b) are fitted to the data points using a version of Eq. (19).

We have therefore estimated Θ_S for the LES cases, by assuming that Stull's heat transfer coefficient, as given by (15), does apply to the LES results. For this purpose, we did a curve fit of Stull's heat transfer coefficient as a function of $\zeta = -Z_i/L$; this is the curve drawn in Fig. 3. We then used (15) to compute Θ_S. We used these values of Θ_S to recompute C_H as defined by Stull. The resulting "corrected" LES C_H and Stull's observed C_H are compared in Fig. 5. The agreement is fair. Obviously, all that this agreement demonstrates is that our curve fit for C_H is reasonably successful. The point is that we can now use this corrected skin temperature to evaluate C_T as defined by (3). This is done in the next section.

TABLE 3. Numerical constants for C_M or C_T curve fits in the form of Eq. (17).

	Unstable	Stable
C_M	$\alpha_1 = -0.016$	$\alpha_1 = -0.027$
	$\alpha_2 = 4.2 \times 10^4$	$\alpha_2 = 2.1 \times 10^2$
	$\alpha_3 = 0.044$	$\alpha_3 = 0.044$
C_T	$\alpha_1 = -0.0195$	$\alpha_1 = -0.016$
	$\alpha_2 = 2.1 \times 10^4$	$\alpha_2 = 8.1 \times 10^2$
	$\alpha_3 = 0.025$	$\alpha_3 = 0.025$

4. The surface transfer coefficients based on the vertically averaged TKE

Figure 6 shows the parameterized bulk turbulent transfer coefficients for heat and momentum, as defined

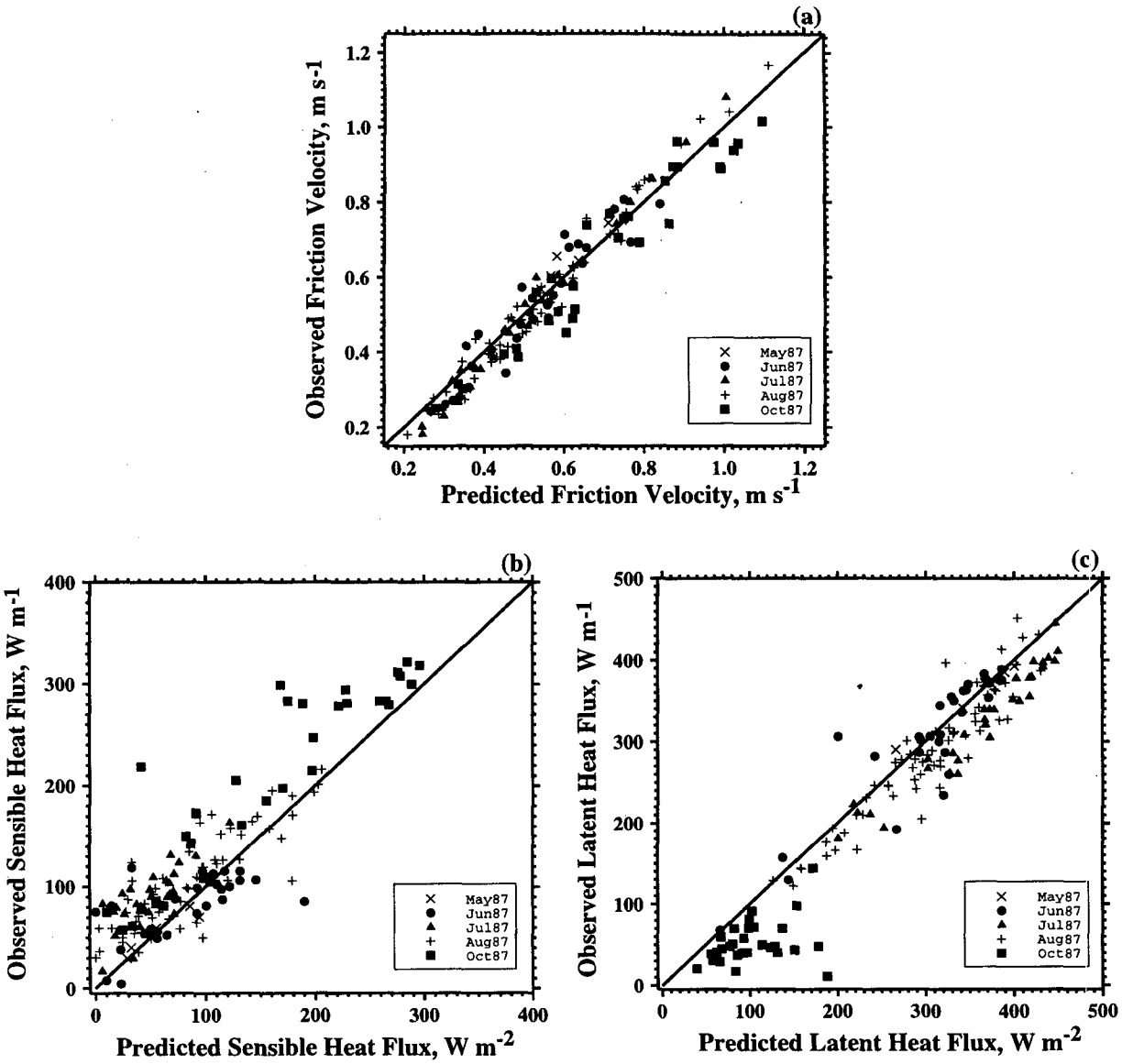

FIG. 7. Comparisons of the predicted surface (a) friction velocity, (b) temperature flux, and (c) moisture flux with independent data obtained at the FIFE site.

by (2) and (3), based on the observations of Stull (1994), the LES results, and data points read from the paper of Lenschow et al. (1988). The transfer coefficients are plotted as functions of a Richardson number based on the square root of the TKE as the velocity scale; that is,

$$\mathrm{Ri}_{\mathrm{TKE}} \equiv -\frac{g(\Theta_{vS} - \Theta_{vM})Z_i}{\Theta_v e_M}, \qquad (16)$$

where Θ_v is the virtual potential temperature. The data plotted in Fig. 6 show that, on the unstable side, with $\mathrm{Ri}_{\mathrm{TKE}} < 0$, both C_M and C_T decrease as conditions become increasingly unstable. This can be explained by considering the budget of the vertically integrated TKE for convective conditions, which can be approximated by a balance between dissipation and buoyant production; that is,

$$\frac{1}{2}\frac{g}{\theta_S}(\overline{w'\theta'})_S Z_i - c(e_M)^{3/2} \approx 0. \qquad (17)$$

Use of (3) in (17) gives

$$C_T \sim \frac{2c}{-\mathrm{Ri}_{\mathrm{TKE}}}. \qquad (18)$$

We thus expect C_T to vary roughly as the inverse of $\mathrm{Ri}_{\mathrm{TKE}}$, under unstable conditions. This is in accord with what we see in Fig. 6.

On the stable side, with $\mathrm{Ri}_{\mathrm{TKE}} > 0$, C_M and C_T decrease quickly to constants as conditions become increasingly stable.

The LES results in Fig. 6 exhibit much less scatter than do Stull's data. According to Stull (1995, personal communication) this may be because the flight legs used to collect the data were too short (on the order of 25 km). It is encouraging that C_M and C_T show so much order when plotted as functions of $\mathrm{Ri}_{\mathrm{TKE}}$. This demonstrates first that variations of $\mathrm{Ri}_{\mathrm{TKE}}$ do affect the values of the transfer coefficients and, second, that the dependence of C_M and C_T on surface roughness is negligible.

We have constructed empirical formulas for C_M and C_T, using functions of the form

$$C_X = \frac{\alpha_1(\mathrm{Ri}_{\mathrm{TKE}})^2}{\alpha_2 + (\mathrm{Ri}_{\mathrm{TKE}})^2} + \alpha_3 = F(\mathrm{Ri}_{\mathrm{TKE}}), \quad (19)$$

where C_X represents either C_M or C_T, and α_1, α_2, and α_3 are numerical constants, whose values are given in Table 3 for stable and unstable conditions, separately. The curves, as shown in Fig. 6, are constructed so that C_M and C_T approach constants for large $|\mathrm{Ri}_{\mathrm{TKE}}|$. For the convective PBL, we expect that $|\mathrm{Ri}_{\mathrm{TKE}}|$ will not become very large, because a large surface–air potential temperature difference (in the numerator) will certainly be associated with a large TKE (in the denominator). On the stable side, however, $|\mathrm{Ri}_{\mathrm{TKE}}|$ could become very large when the surface is radiatively cooled, with weak turbulent mixing.

We have tested our parameterization using an independent dataset, based on the First International Satellite Land Surface Climatology Project (ISLSCP) Field Experiment (FIFE) campaign, which was conducted during May, June, July, August, and October of 1987 and 1989 (Sellers et al. 1992). The FIFE site covered a 15 km × 15 km, homogeneous grassland located near Manhattan, Kansas (39°N, 96°W). Ac-

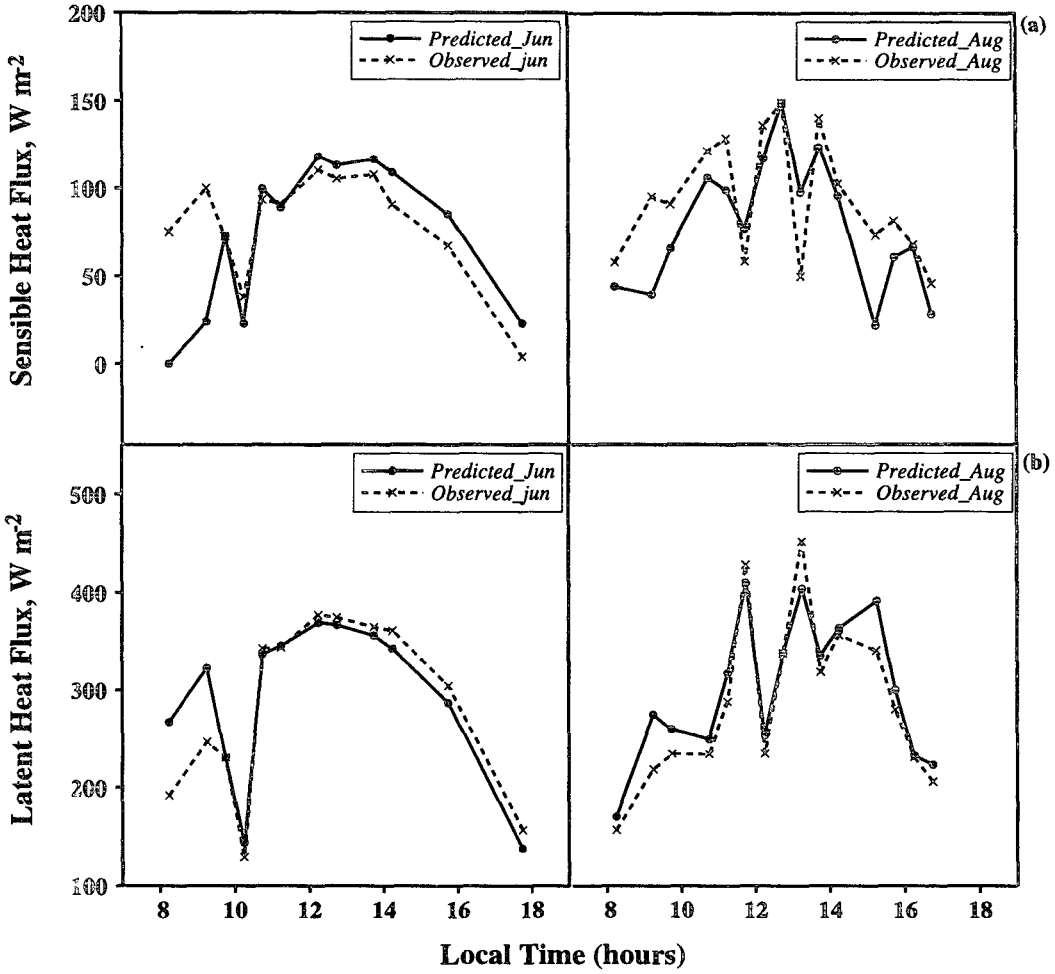

FIG. 8. Comparisons of the composite diurnal cycles of surface (a) sensible and (b) latent heat fluxes, between the predictions and the observations in June and August of 1987.

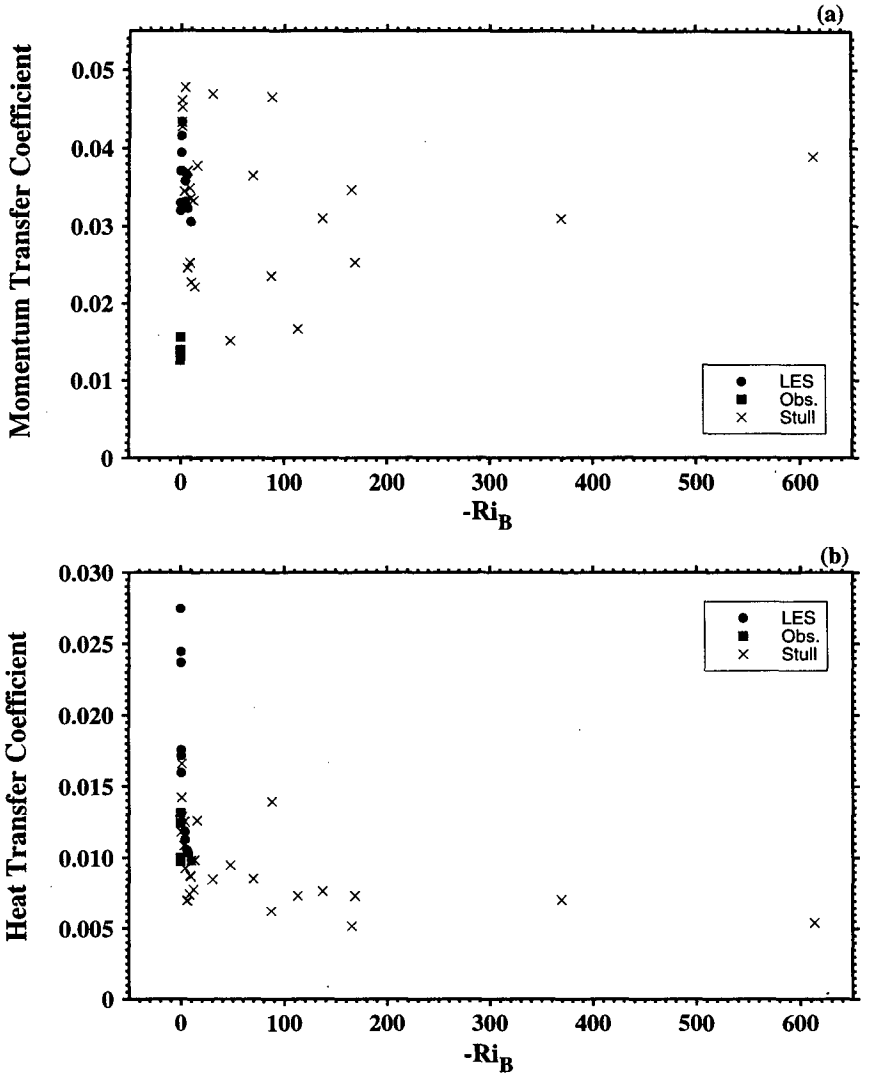

FIG. 9. Plots of the surface transfer coefficients as functions of the bulk Richardson number.

cording to Sugita and Brutsaert (1992), the surface roughness length is close to 1.05 m.[2] We used data only from the 1987 FIFE field campaign. The observed mean profiles, surface radiative temperature, and surface turbulent fluxes were used to test our surface transfer coefficient parameterization, as given by (19). The mean profiles of wind, potential temperature, and water vapor mixing ratio were measured using radiosondes launched from the northern edge of the FIFE site (Sugita and Brutsaert 1990; Brutsaert and Sugita 1990, 1991). The PBL depth was estimated from the mean profiles of the potential temperature and water vapor mixing ratio. During the profile measurements, the mean wind blew from the south over the FIFE site, so that the radiosonde measurements were located downwind from the surface flux and meteorological stations. The surface radiative (skin) temperature was measured by nadir-looking infrared radiation thermometers at four "super automatic meteorological" stations distributed within the FIFE site. The 30-min mean skin temperatures at these four stations were then averaged to give the area-averaged skin temperature. The surface turbulent fluxes were measured using either eddy correlation or Bowen ratio stations distributed over the FIFE site. We used data from eight such stations, and

[2] Betts and Beljaars (1993) and Beljaars (1994) also calculated the surface roughness lengths for FIFE and BLX83, respectively. Their results (0.19 m for FIFE and 0.34 m for BLX83) are somewhat different from those reported by Sugita and Brutsaert (1992) and Stull (1994).

averaged their 30-min mean fluxes to represent the area-averaged surface fluxes. The mean profiles of wind, temperature, and humidity were then synchronized to produce a consistent time series. We took the data as given, without any additional quality control, such as selecting particular wind directions or atmospheric stability conditions. During the FIFE campaign, there were periods of bad weather, rain, and persistent cloud cover at the field site (Sellers et al. 1992). We used the data regardless of the weather conditions.

Figure 7 shows comparisons of the predicted surface friction velocity, temperature flux, and moisture flux with the FIFE observations. A total of 158 data points representing 30-min means are used in the comparisons. The predicted momentum and temperature fluxes are based on calculations using the bulk transfer parameterization C_M and C_T in (2), (3), and (19). Direct estimation of the latent heat flux is not attempted here because we would need information on soil wetness and transpiration in order to predict the latent heat fluxes using (4) and (19). Instead, we diagnose the latent heat flux as a residual of the surface energy budget; that is,

$$\mathrm{LE}_p = \mathrm{RN}_o - (H_p + G_o), \tag{20}$$

where RN is surface net radiation, H is the sensible heat flux, LE is the latent heat flux, and G is the soil heat flux. The subscript o denotes observations and subscript p denotes calculations.

Because we have no measured values of the surface friction velocity, we have estimated the "observed"

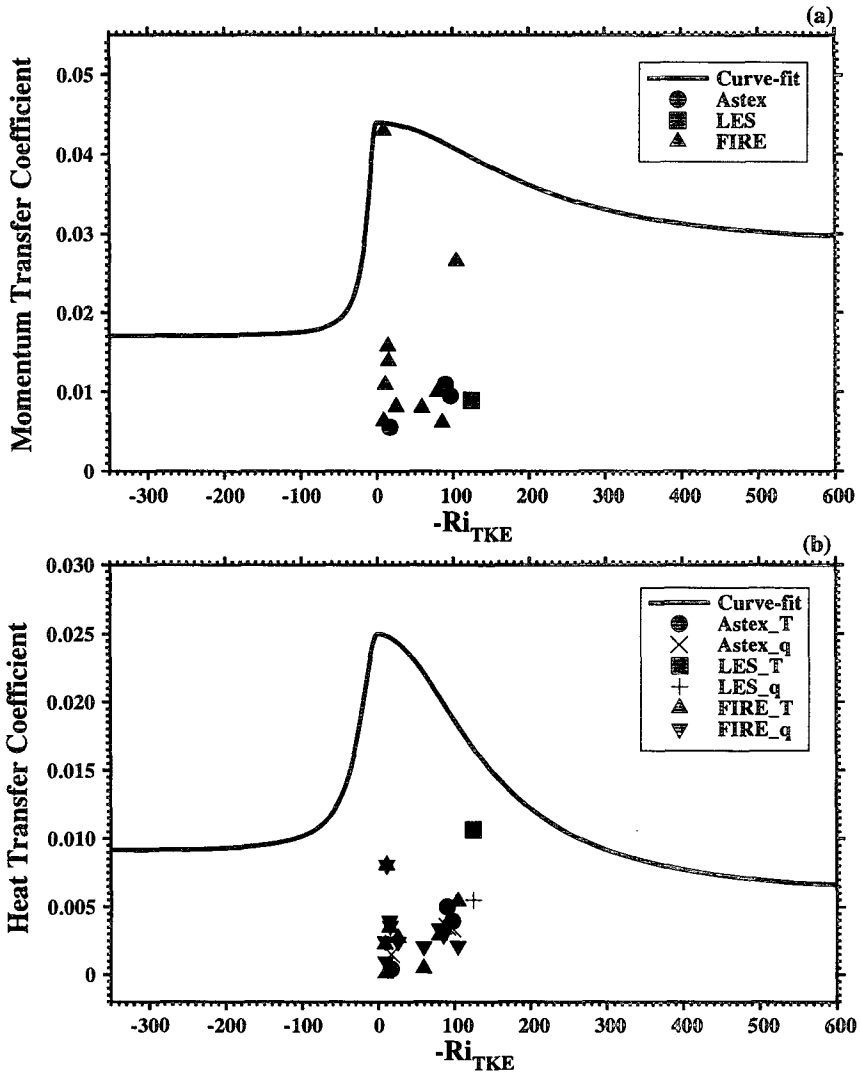

FIG. 10. Comparisons of the calculated (a) C_M and (b) C_T for the stratocumulus-topped boundary layer cases, plotted together with the curve fit (19) based on clear-sky data.

friction velocity shown in Fig. 7a by using the log-profile relationship:

$$u_* = kU_m\left[\ln\left(\frac{Z_m}{z_0}\right) + \Psi_M\left(\frac{Z_m}{L}\right)\right]^{-1}, \quad (21)$$

where $Z_m = Z_i/2$, L is the Monin–Obukhov length and Ψ_M is the empirical stability correction for log-wind profile. We use Ψ_M as given by Paulson (1970). Brutsaert and Sugita (1991) calculated the surface friction velocity at the FIFE site by a similar method.

As shown in Fig. 7a, the parameterized friction velocity obtained from (2) and (19) agrees very well with the observed friction velocity. On average, the ratio of the parameterized u_* to that observed is 1.02; the mean relative error of the parameterized u_* with respect to the observed is 2.27%; and the correlation coefficient between the observed and computed values of u_* is 0.971. We note that this good agreement is obtained without taking into account any possible roughness dependence of our transfer coefficients.

The predicted surface sensible heat fluxes (H_p) also agree well with the corresponding observed fluxes (H_o), as shown in Fig. 7b, although the predicted values are somewhat smaller than the observed. On the other hand, the predicted values generally are larger than observed for surface latent heat flux. This is partially due to the errors of the TKE as diagnosed by Eq. (10). As shown in Fig. 2, the diagnosed TKEs are less than the LES values for the weak-turbulence cases and larger for the strong-turbulence cases. Each data point represents an average over a 30-min interval. This averaging time may be too short compared with the typical interval between the passage of large organized convective eddies. The mean ratio of the parameterized to the observed sensible heat flux is 0.81; the mean relative error is 19.4%; and the correlation coefficient is 0.84.

Figure 7c shows good agreement between the parameterized and observed latent heat fluxes. The differences between them are influenced by the accuracy of the sensible heat flux predictions. The mean ratio is 1.09; the mean relative error is 8.99%; and the correlation coefficient is 0.94.

Figure 8 compares the composited diurnal cycles of the sensible (a) and latent (b) heat fluxes, as parameterized and observed, for data obtained in June and August 1987 at the FIFE site. The parameterized fluxes follow the observations very well, especially for the convective PBL during late morning and afternoon at the local time. There are larger differences between the predictions and observations for both H and LE in the earlier morning hours. There are strong variations of the composite diurnal cycles of H and LE between consecutive observation hours in August, suggesting that there were either large organized convective eddies or cloud shading at FIFE site during this period. The parameterized surface fluxes, however, reflected the observed conditions.

We have also plotted our transfer coefficients against a more conventional measure of stability, the "bulk Richardson number" as used, for example, by Deardorff (1972):

$$\mathrm{Ri}_B \equiv -\frac{g(\Theta_{vS} - \Theta_{vM})Z_i}{\Theta_v U_M^2}. \quad (22)$$

This differs from (16) only in that the square of the PBL-mean wind appears in the denominator, in place of the TKE. The results are shown in Fig. 9. The heat transfer coefficient varies with Ri_B in a somewhat orderly way, but the momentum transfer coefficient does not seem to recognize the value of Ri_B at all.

The significant dependence of the transfer coefficients on stability, as found here, differs from the results of Businger and Oncley (1990), who used a near-surface vertical velocity variance in place of e_M, and found little dependence of the resulting transfer coefficients on stability. Unfortunately, the approach of Businger and Oncley (1990) cannot be used in a numerical model with coarse vertical resolution, because such a model cannot predict the vertical velocity variance in the surface layer. Our approach is in principle compatible with that of Businger and Oncley, however. By combining their results with ours, one could deduce a relationship between the near-surface vertical velocity variance and the vertically integrated TKE.

Such a relationship might be expected to depend on the presence of clouds within the PBL. The reason is that substantial TKE production can occur within such cloud layer, well above the surface, and at a rate that is only indirectly linked to the surface fluxes (e.g., Lilly 1968). This suggests that the values of the transfer coefficients defined by (2)–(4) could be significantly altered by the presence of boundary layer clouds. Figure 10 shows C_M and C_T as calculated using observations of the stratocumulus-topped marine boundary layer from the Atlantic Stratocumulus Transition Experiment—ASTEX (Wang and Lenschow 1995), from the 1987 marine stratocumulus portion of FIRE (Moyer and Young 1993) and from an LES simulation of a stratocumulus-topped boundary layer case (Moeng et al. 1996). A summary of the stratocumulus-topped boundary layer data is given in Table 4. Although $\mathrm{Ri}_{\mathrm{TKE}}$ as defined by (16) is not very relevant to the stratocumulus-topped boundary layer, the values of C_M and C_T shown in Fig. 10 are considerably smaller than those given by the curve fit based on the clear-sky convective boundary layer data, for most values of $\mathrm{Ri}_{\mathrm{TKE}}$. We tentatively conclude that the vertically averaged TKE for such stratocumulus cases, which is strongly influenced by buoyancy generation in the elevated cloud layer, is "too large" for use with the transfer coefficients that apply to the clear-sky case. Further research is needed to parameterize the transfer coefficients for the case of stratocumulus-topped boundary layers.

TABLE 4. Summary of the datasets for stratocumulus cloud cases.

Data source	Cases	Z_i (m)	U_M (m s^{-1})	Θ_{vM} (K)	Q_M (g kg^{-1})	Θ_{vS} (K)	Surface buoyancy flux (K m s^{-1})	Surface moisture flux (g m kg^{-1} s^{-1})	u_* (m s^{-1})	e_M (m^2 s^{-2})	Ri_B
LES	1	752	4.37	290.7	7.8	292.0	0.0074	0.1431	0.1431	0.2739	−1.789
ASTEX	1	600	9.27	291.3	9.8	291.8	0.0002	0.0030	0.1982	0.5798	−0.1121
	2	700	10.21	291.0	9.8	293.7	0.0084	0.0116	0.2786	0.6405	−0.5960
	3	1100	8.75	293.7	10.0	295.2	0.0059	0.0146	0.2736	0.6117	−0.7212
FIRE	1	1021	5.77	292.3	9.5	292.6	0.0084	0.0170	0.1710	0.3854	−0.2955
	2	914	4.34	291.4	9.7	292.7	0.0018	0.0187	0.1680	0.6603	−2.077
	3	853	9.34	291.5	8.8	291.8	0.0098	0.0271	0.2421	0.9769	−0.0959
	4	914	10.83	291.1	8.2	291.5	0.0148	0.0342	0.3544	0.6984	−0.0905
	5	700	13.59	290.8	9.7	291.1	0.0055	0.0250	0.3857	0.4796	−0.0371
	6	640	13.93	289.2	9.3	289.6	0.0000	0.0068	0.3389	0.5702	−0.0323
	7	940	7.35	291.4	9.7	292.8	0.0117	0.0243	0.1819	0.5404	−0.8546
	8	792	7.68	291.7	10.2	293.6	0.0193	0.0172	0.3749	0.4762	−0.8433
	9	792	2.34	290.6	10.0	291.0	0.0003	0.0078	0.3029	0.8327	−1.421
	10	1151	7.90	290.6	7.6	291.7	0.0131	0.0308	0.2412	0.5447	−0.6977

5. Conclusions

A new bulk transfer formulation for the surface turbulent fluxes of momentum, heat, and moisture has been developed using the square root of the vertically averaged turbulence kinetic energy as a velocity scale, in place of the mean wind speed. The new parameterization utilizes the surface radiative skin temperature, instead of the roughness-height temperature. We used both field observations and large-eddy simulations in the development of the parameterization.

The parameterization has been tested using an independent dataset from the First ISLSCP (International Satellite Land Surface Climatology Project) Field Experiment (FIFE). The parameterized surface momentum flux compares very well with the observations despite the fact that the dataset used for developing the parameterization has a very different surface roughness length from the independent FIFE data, indicating that the parameterization can represent a wide range of surface roughness boundary conditions. The predicted sensible and latent heat fluxes also agree well with the FIFE observations, although the predicted surface sensible heat flux is somewhat smaller than observed. The predicted diurnal cycles of the surface sensible heat and latent heat fluxes correspond very well with the observations in both magnitude and phase.

The results reported here do not show a significant dependence of our transfer coefficients on the surface roughness. More data for a wider range of conditions are needed to explore this issue further. Clear-sky data over the oceans would be particularly useful.

We have also presented some evidence that the transfer coefficients defined by (2)–(4) are considerably reduced in the presence of boundary layer clouds. The influence of cloudiness on the surface turbulent exchange is a subject that has not been adequately explored, and we view this as a fruitful area for further research.

Acknowledgments. The FIFE data was obtained through the FIFE information system and the Pilot Land Data System (PLDS). This work has been supported by NASA's Earth Observation System (EOS) program, through the Sellers-Mooney Interdisciplinary Science Project under NASA Contract NAS5-31730, by NASA's FIRE program under Grant NAG1-1701, and by the U.S. Department of Energy's CHAMMP program under Grant DE-FG03-94ER61929, all to Colorado State University. Computing resources were provided by NASA's Center for Computational Sciences.

REFERENCES

Beljaars, A. C. M., 1995: The parameterization of surface fluxes in large scale models under free convection. *Quart. J. Roy. Meteor. Soc.*, **121,** 255–270.

——, and A. M. Holtslag, 1991: Flux parameterization over land surfaces for atmospheric models. *J. Appl. Meteor.*, **30,** 327–341.

Betts, A. K., and A. C. M. Beljaars, 1993: Estimation of effective roughness length for heat and momentum from FIFE data. *Atmos. Res.*, **30,** 251–261.

Brutsaert, W., and M. Sugita, 1990: The extent of the unstable Monin–Obukhov layer for temperature and humidity above complex hilly grassland. *Bound.-Layer Meteor.*, **51,** 383–400.

——, and ——, 1991: A bulk similarity approach in atmospheric boundary layer using radiometric skin temperature to determine regional surface fluxes. *Bound.-Layer Meteor.*, **55,** 1–23.

——, and ——, 1992: Regional surface fluxes from satellite-derived surface temperatures (AVHRR) and radiosonde profiles. *Bound.-Layer Meteor.*, **58,** 355–366.

Businger, J. A., and S. P. Oncley, 1990: Flux measurement with conditional sampling. *J. Atmos. Oceanic Technol.*, **7,** 349–352.

——, J. C. Wyngaard, Y. Izumi, and E. F. Bradley, 1971: Flux profile relationships in the atmospheric surface layer. *J. Atmos. Sci.*, **28,** 181–189.

Caughey, S. J., J. C. Wyngaard, and J. C. Kaimal, 1979: Turbulence in the evolving stable boundary layer. *J. Atmos. Sci.*, **36,** 1041–1052.

Choudhury, B., 1985: A note on canopy and air temperature equality. *Agric. Meteor.*, **34,** 333–336.

Deardorff, J. A., 1970: Convective velocity and temperature scales for the unstable planetary boundary layer and for Rayleigh convection. *J. Atmos. Sci.*, **27,** 1211–1213.

——, 1972: Parameterization of the planetary boundary layer for use in general circulation models. *Mon. Wea. Rev.*, **100,** 93–106.

Driedonks, A. G. M., 1982: Models and observations of the growth of the atmospheric boundary layer. *Bound.-Layer Meteor.*, **23,** 283–306.

Dyer, A. J., 1974: A review of flux-profile relations. *Bound.-Layer Meteor.*, **1,** 363–372.

Garratt, J. R., 1977: Review of drag coefficients over ocean and continents. *Mon. Wea. Rev.*, **105,** 912–928.

——, 1992: *The Atmospheric Boundary Layer.* Cambridge Atmospheric and Space Science Series, Cambridge University Press, 316 pp.

——, and R. J. Francey, 1978: Bulk characteristics of heat transfer in the unstable baroclinic atmospheric boundary layer. *Bound.-Layer Meteor.*, **15,** 3995–421.

Godfrey, J. S., and A. C. M. Beljaars, 1991: On the turbulent fluxes of buoyancy, heat and moisture at air–sea interface at low wind speeds. *J. Geophys. Res.*, **96,** 22 043–22 048.

Kondo, J., 1975: Air–sea bulk transfer coefficients in diabatic conditions. *Bound.-Layer Meteor.*, **9,** 91–112.

Langlois, W. E., and H. C. W. Kwok, 1969: Description of the Mintz–Arakawa Numerical General Circulation Model. Numerical Simulation of Weather and Climate Tech. Rep. 3, 95 pp. [Available from Department of Atmospheric Science, University of California, Los Angeles, Los Angeles, CA 90095.]

Lenschow, D. H., X. S. Li, and C. J. Zhu, 1988: Stably stratified boundary layer over the great plains. Part I: Mean and turbulent structure. *Bound.-Layer Meteor.*, **42,** 95–121.

Lilly, D. K., 1968: Models of cloud-topped mixed layers under a strong inversion. *Quart. J. Roy. Meteor. Soc.*, **94,** 292–309.

Liu, W. T., L. B. Katsaros, and J. A. Businger, 1979: Bulk parameterization of air–sea exchanges of heat and water vapor including the molecular constraints at interface. *J. Atmos. Sci.*, **36,** 1722–1735.

Louis, J. F., 1979: A parametric model of vertical eddy fluxes in the atmosphere. *Bound.-Layer Meteor.*, **17,** 187–202.

Mahrt, L., and J. Sun, 1995: The subgrid velocity scale in the bulk aerodynamic relationship for spatially averaged scalar fluxes. *Mon. Wea. Rev.*, **123,** 3032–3043.

Miller, M. J., A. C. M. Beljaars, and T. N. Palmer, 1992: The sensitivity of the ECMWF model to the parameterization of evaporation from the tropical ocean. *J. Climate,* **5,** 418–434.

Moeng, C.-H., 1984: A large-eddy-simulation model for study of planetary boundary layer turbulence. *J. Atmos. Sci.*, **41,** 2052–2062.

——, and J. C. Wyngaard, 1988: Spectral analysis of large-eddy simulations of the convective boundary layer. *J. Atmos. Sci.*, **45,** 3575–3587.

——, and P. P. Sullivan, 1994: A comparison of shear- and buoyancy-driven planetary boundary flows. *J. Atmos. Sci.*, **51,** 999–1022.

——, and Coauthors, 1996: Simulation of a stratocumulus-topped PBL: Intercomparison among different numerical codes. *Bull. Amer. Meteor. Soc.*, **77,** 261–278.

Moyer, K. A., and G. S. Young, 1993: Buoyant forcing within the marine stratocumulus-topped boundary layer. *J. Atmos. Sci.*, **50,** 2759–2771.

Paulson, C. A., 1970: The mathematical representation of wind speed and temperature in the unstable atmospheric surface layer. *J. Appl. Meteor.*, **9,** 857–861.

Paw U, K. T., 1984: A theoretical basis for the leaf equivalence point temperature. *Agric. Meteor.*, **30,** 247–256.

Randall, D. A., 1976: The interaction of the planetary boundary layer with large-scale circulations. Ph.D. thesis, University of California, Los Angeles, 247 pp.

Sellers, P. J., F. G. Hall, G. Asrar, D. E. Strebel, and R. E. Murphy, 1992: An overview of the First International Satellite Land Surface Climatology Project (ISLSCP) Field Experiment (FIFE). *J. Geophys. Res.*, **97,** 18 345–18 371.

Sommeria, G., 1988: Parameterization of the planetary layer in large-scale atmospheric models. *Physically-based Modeling and Simulation of Climate and Climatic Change—Part 1.* M. E. Schlesinger, Ed., Kluwer Academic Publishers, 331–374.

Stewart, J. B., 1995: Turbulent surface fluxes derived from radiometric surface temperature of sparse prairie grass. *J. Geophys. Res.*, **100,** 25 429–25 433.

Stull, R. B., 1988: *An Introduction to Boundary Layer Meteorology.* Kluwer Academic Publishers, 666 pp.

——, 1994: A convective transport theory for surface fluxes. *J. Atmos. Sci.*, **51,** 3–22.

Suarez, M. J., A. Arakawa, and D. A. Randall, 1983: The parameterization of the planetary boundary layer in the UCLA general circulation model: Formulation and results. *Mon. Wea. Rev.*, **111,** 2224–2243.

Sugita, M., and W. Brutsaert, 1990: Wind velocity measurements in neutral boundary layer above hilly prairie. *J. Geophys. Res.*, **95,** 7617–7624.

——, and ——, 1992: The stability functions in the bulk similarity formulation for the unstable boundary layer. *Bound.-Layer Meteor.*, **61,** 65–80.

Sun, J., and L. Mahrt, 1995: Determination of surface fluxes from the surface radiative temperature. *J. Atmos. Sci.*, **52,** 1096–1106.

Tennekes, H., 1973: A model for the dynamics of the inversion above a convective boundary layer. *J. Atmos. Sci.*, **30,** 558–567.

Thom, A. S., 1972: Momentum, mass and heat exchange of vegetation. *Quart. J. Roy. Meteor. Soc.*, **98,** 124–134.

Wang, Q., and D. H. Lenschow, 1995: An observational study of the role of penetrating cumulus in a marine stratocumulus-topped boundary layer. *J. Atmos. Sci.*, **52,** 2778–2787.

Yamada, T., 1976: On the similarity functions A, B and C of the planetary boundary layer. *J. Atmos. Sci.*, **33,** 781–793.